

CO³: Cooperative Unsupervised 3D Representation Learning for Autonomous Driving

Runjian Chen
The University of Hong Kong
rjchen@connect.hku.hk

Yao Mu
The University of Hong Kong
muyao@connect.hku.hk

Runsen Xu
Zhejiang University
runsenxu@zju.edu.cn

Wenqi Shao
The Chinese University of Hong Kong
weqish@link.cuhk.edu.hk

Chenhan Jiang
Huawei Noah's Ark Lab
jiang.chenhan@huawei.com

Hang Xu
Huawei Noah's Ark Lab
xu.hang@huawei.com

Zhenguo Li
Huawei Noah's Ark Lab
li.zhenguo@huawei.com

Ping Luo
The University of Hong Kong
pluo@cs.hku.hk

Abstract: Unsupervised contrastive learning for indoor-scene point clouds has achieved great successes. However, unsupervised representation learning on outdoor-scene point clouds remains challenging because previous methods need to reconstruct the whole scene and capture partial views for the contrastive objective. This is infeasible in outdoor scenes with moving objects, obstacles, and sensors. In this paper, we propose **CO³**, namely **Cooperative Contrastive Learning and Contextual Shape Prediction**, to learn 3D representation for outdoor-scene point clouds in an unsupervised manner. **CO³** has several merits compared to existing methods. (1) It utilizes LiDAR point clouds from vehicle-side and infrastructure-side to build views that differ enough but meanwhile maintain common semantic information for contrastive learning, which are more appropriate than views built by previous methods. (2) Alongside the contrastive objective, contextual shape prediction is proposed as pre-training goal and brings more task-relevant information for unsupervised 3D point cloud representation learning, which are beneficial when transferring the learned representation to downstream detection tasks. (3) As compared to previous methods, representation learned by **CO³** is able to be transferred to different outdoor scene dataset collected by different type of LiDAR sensors. (4) **CO³** improves current state-of-the-art methods on both *Once* and *KITTI* datasets by up to 2.58 mAP. Codes and models will be released. We believe **CO³** will facilitate understanding LiDAR point clouds in outdoor scene.

1 Introduction

As the most reliable sensor in outdoor environments, LiDAR is able to precisely measure 3D location of objects and both of the robotics and computer vision communities have shown strong interest on perception tasks on LiDAR point clouds, including 3D object detection, segmentation and tracking, which are essential to autonomous driving system. Up to now, randomly initializing and directly *training from scratch* on detailed annotated data still dominates this field. On the contrary, recent research efforts [1, 2, 3, 4, 5] in image domain focus on unsupervised representation learning with contrastive objective on different views built from images (the first column of Figure 1 shows example views built by [1, 2, 3, 4, 5]). They pre-train the 2D backbone with a large-scale dataset like ImageNet [6] in an unsupervised manner and use the pre-trained backbone to initialize downstream neural networks on different datasets, which achieve significant performance improvement over *training from scratch* in 2D object detection [7, 8, 9]. Inspired by these successes together with the abundant unlabelled data available from self-driving vehicles, we explore unsupervised representation learning for *outdoor scene* point clouds to improve the performance on 3D object detection tasks.

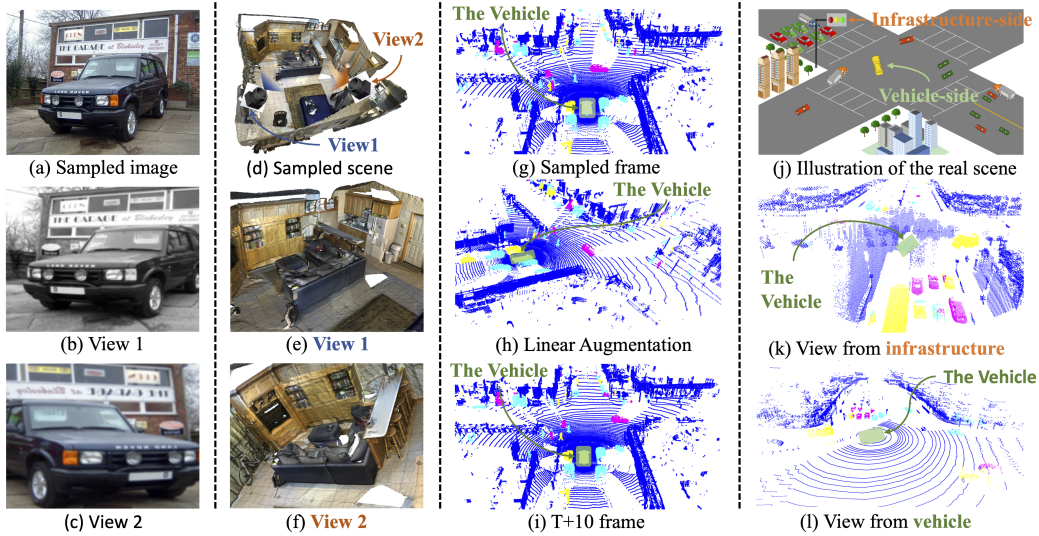


Figure 1: Example views built by different methods in contrastive learning. (a), (b) and (c) are sampled image and views (different augmentations of the original image) used in [1, 2, 3, 4, 5]. (d), (e) and (f) show an example of two views built in PointContrast [11], which are captured at different poses in the reconstructed point clouds (d). Views built in this way differ much but meanwhile still maintain enough common semantic information including the same sofa and table. (g) and (h) are views for outdoor-scene point cloud from [15]. (g) is the original frame of point cloud and authors in [15] apply point cloud augmentation to (g) for (h), which can be implemented with a simple linear transformation. [16] use point cloud at different timestamps as views for contrastive learning, which are indicated in (g) and (i). The autonomous vehicle is waiting at the crossing while other cars and pedestrians are moving around, making it hard to find accurate correspondence for contrastive learning. (j) is an illustration of the sampled real scene and (k), (l) are views from vehicle and infrastructure sides, which are used by CO³ to make views more suitable for contrastive learning.

In the past decade, learning 3D representation from unlabelled data has achieved great success in *single-object* and *indoor-scene* point clouds. For point clouds of *single objects* such as CAD models, previous works pre-train 3D encoders to predict a **global** representation by minimizing contrastive loss [10] and aim at low-level downstream tasks including object classification and registration. To extend this idea to high-level perception tasks for *indoor-scene* point clouds, PointContrast [11] propose to reconstruct the whole indoor scenes, collect partial point clouds from two different poses and utilize them as two views in contrastive learning to learn **dense** (point-level or voxel-level) representation. More recent works such as [12] and [13] also need the reconstruction and this naturally assumes that the environment is static. Figure 1 (d), (e) and (f) show examples of views in PointContrast [11]. We can see that the views differ a lot because they are captured from different poses but meanwhile, they still contain enough common semantic information such as the same sofa and table, which are demonstrated important property of views in contrastive learning in [14].

However, outdoor scenes are dynamic and large-scale, making it impossible to reconstruct the whole scenes for building views. Thus, methods in [11, 12, 13] cannot be directly transferred but there exists two possible alternatives to build views. The first idea, embraced by [15], is to apply data augmentation to single frame of point cloud and treat the original and augmented versions as different views, as indicated by Figure 1 (g) and (h). However, all the augmentation of point clouds, including random drop, rotation and scaling, can be implemented in a linear transformation and views constructed in this way do not differ enough. The second one is to consider point clouds at different timestamps as different views, represented by [16]. Yet the moving objects would make it hard to find correct correspondence for contrastive learning. See Figure 1 (g) and (f), while the autonomous vehicle is waiting for the traffic light to turn green, other cars and pedestrians are moving. The autonomous vehicle has no idea about how they move and is not able to find correct correspondence (common semantics). Due to these limitations, pre-trained 3D encoders in [15, 16] cannot achieve noticeable improvement when transferring to datasets collected by different LiDAR sensors.

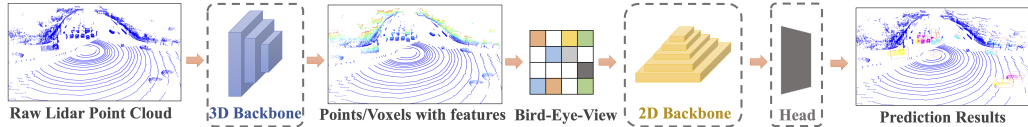


Figure 2: Summary of 3D object detectors. The raw input LiDAR point cloud is first processed by the 3D backbone and per-point/voxel representations are generated, which are further transformed into the Bird-Eye-View (BEV) map. Finally, a 2D backbone and a detection head are applied to generate the detection results.

To overcome these limitations, we propose **CO**operative **CO**ntrastive Learning and **CO**ntextual Shape Prediction, **CO³**, to learn representation for outdoor-scene point clouds in an unsupervised manner. **CO³** mainly contains two components, as described below.

Cooperative Views for Contrastive Learning. To build views of LiDAR point clouds that differ enough and share adequate semantic information, we propose to utilize a recently released infrastructure-vehicle-cooperation dataset called DAIR-V2X [17] and build views for contrastive representation learning using point clouds respectively from infrastructure LiDAR and vehicle LiDAR. As shown in (j), (k) and (l) in Figure 1, views built in this way differ a lot because they are captured at different positions and they share enough information because they are captured at the same timestamp. With the raw input point clouds from the vehicle and infrastructure, we further fuse the point cloud from both sides at the same timestamp and use the fusion point cloud and point cloud from vehicle-side as two views in contrastive representation learning. Background information about view building in contrastive learning can be found in Appendix A.

Contextual Shape Prediction. As proposed in [18], representation learned from purely contrastive learning is not able to capture task-relevant information and a reconstruction objective can be implemented alongside to compensate this limitation (for more details, please refer to Appendix B). Detailed experiments on image representation learning have been conducted in [18] to demonstrate this statement and we want to borrow this idea to 3D point cloud. However, it can be extremely difficult to reconstruct the whole scene with point-level or voxel-level representations. Instead, we propose a pre-training goal to reconstruct local distribution of neighboring points using the dense representations. In practice, we use shape context to describe the local distribution of each point’s neighborhood, which has been demonstrated as a useful local distribution descriptor in previous works [12, 19, 20, 21].

Figure 3 shows two examples of shape context with 8 bins (the number of bins can be changed). The neighborhood of the query point (marked as a larger black point) is first divided into 8 bins and we compute an 8-dimensional distribution with the numbers of points in these bins. The pre-training task is to predict local distributions of each point or voxel with the extracted point-level or voxel-level representation. This refined reconstruction pre-training task introduces more task-relevant information and helps learn much better representations.

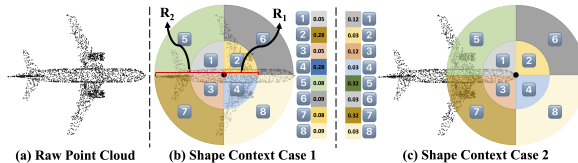


Figure 3: Two examples of shape context.

Our contributions can be summarized as follows. (1) **CO³** is proposed to utilize the vehicle-infrastructure-cooperation dataset to build adequate views for unsupervised contrastive 3D representation learning on *outdoor-scene* point clouds. (2) A shape-context prediction task is proposed alongside to inject task-relevant information, which is beneficial for downstream 3D detection tasks. (3) The learned 3D representations can be well transferred to datasets collected by different LiDAR sensors. (4) Extensive experiments demonstrate the effectiveness of **CO³**. For example, **CO³** improves Second, PV-RCNN, CenterPoints on *Once* [22] by 1.07, 0.62 and 2.58 respectively.

2 Related Works

3D Object Detection. Figure 2 summarizes current 3D object detection methods in autonomous driving scenes. The raw LiDAR point clouds is first passed through a 3D encoder and transferred into per-point or per-voxel representation. Then these dense representation is projected onto the ground plane and we get Bird-Eye-View (BEV) map. After that, the BEV map is encoded by a 2D backbone

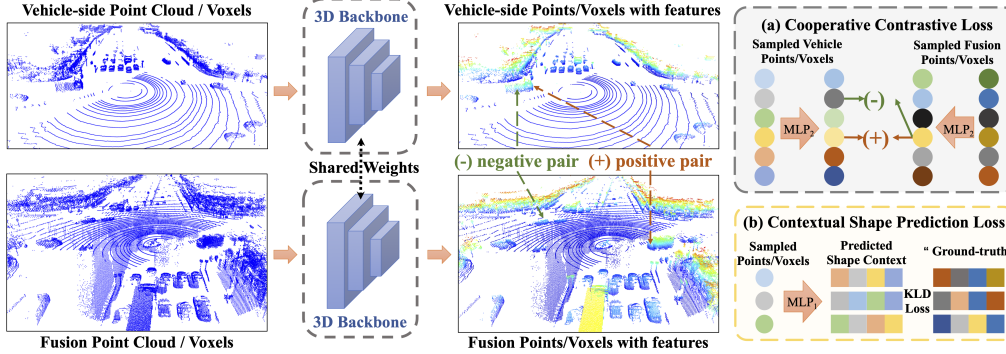


Figure 4: The pipeline of CO^3 . The infrastructure point cloud is transformed and fused with vehicle point cloud beforehand. With vehicle-side and fusion point clouds as inputs, we first process them with the 3D backbone to generate point/voxel-level representations. With these dense representations, we propose two pre-training objectives: (a) Cooperative Contrastive Loss, which introduces adequate views for contrastive learning. (b) Contextual Shape Prediction Loss, to bring in task-relevant information that are beneficial for downstream tasks.

followed with a detection head and the final detection results are generated. Up to now, 3D object detectors can be divided into three main streams due to different 3D encoders they use: (1) point-based methods [23, 24, 25] use point-based 3D backbone. (2) voxel-based methods [26, 27, 28, 29, 30, 31] generally transform point cloud into voxel grids and process them using 3D volumetric convolutions. (3) point-voxel-combined methods [32, 33, 34] utilize features from both (1) and (2). Among all these methods, [26, 30, 33] are the most widely used detectors and achieve state-of-the-art performance. However, all these methods rely on precise 3D annotations and we propose CO^3 to pre-train 3D backbones without labels for outdoor-scene LiDAR point clouds.

Unsupervised 3D Representation Learning for LiDAR Point Clouds. Contrastive pre-training on different views of images have demonstrated promising performance in image domain [1, 2, 3, 4, 5] and PointContrast [11] is the pioneering work for unsupervised contrastive learning on *indoor-scene* point clouds. Together with the following works including [12, 13], they rely on the assumption of static scenes that have been registered for constructing adequate views. To extend their ideas to outdoor-scene LiDAR point clouds, [15] augment single frame of point cloud to build views and [16] utilizes point clouds at different timestamps as views for unsupervised contrastive learning. However, as discussed in section 1, the views built in [15] are too similar while those in [16] are hard to find correct correspondence, which violate the property for adequate views in contrastive learning as proposed in [14] and make their representations unable to transfer to datasets collected by different LiDAR sensors. In this work, we propose to use point clouds from vehicle and infrastructure to construct views in contrastive learning and introduce task-relevant information with a shape-context prediction pre-training goal to learn better 3D representation.

3 Methods

In this section, we introduce the proposed CO^3 for unsupervised representation learning on LiDAR point clouds in outdoor scenes. As detailed in Figure 4, CO^3 has two pre-training objectives: (a) a cooperative contrastive learning goal on dense (point-level or voxel-level) representations between vehicle-side and fusion point clouds, which provides adequate views for contrastive learning. (b) a contextual shape prediction loss to bring in more task-relevant information. To start with, we discuss the problem formulation and overall pipeline in Section 3.1. Then we respectively introduce the cooperative contrastive objective and contextual shape prediction goal in Section 3.2 and Section 3.3.

3.1 Problem Formulation and Pipeline

To begin with, we define the raw LiDAR point clouds from vehicle-side and infrastructure-side respectively as $\mathbf{P}_{\text{veh}} = [\mathbf{P}_{\text{veh}}^{\text{xyz}}, \mathbf{P}_{\text{veh}}^{\text{feat}}]$ and $\mathbf{P}_{\text{inf}} = [\mathbf{P}_{\text{inf}}^{\text{xyz}}, \mathbf{P}_{\text{inf}}^{\text{feat}}]$, where $\mathbf{P}_{v/i}^{\text{xyz}} \in \mathbb{R}^{N_{v/i}^p \times 3}$ and $\mathbf{P}_{v/i}^{\text{feat}} \in \mathbb{R}^{N_{v/i}^p \times d}$. Here $N_{v/i}^p$ denotes the number of points (or voxels) in vehicle-side and infrastructure-side respectively and $d = 1$ is always the case to represent the intensity of each point (or voxel). **Note** here that as vehicle/infrastructure/fusion point clouds may sometimes go through the same process, we will change the notation to $v/i/f$ to indicate the same processing on respective point cloud for convenience.

When collecting the cooperative dataset, each pair of vehicle-side and infrastructure-side point clouds is associated with a transformation $T_{\text{inf}}^{\text{veh}}$ indicating the relationship between vehicle-side coordinate and infrastructure-side coordinate.

With \mathbf{P}_{veh} , \mathbf{P}_{inf} and $T_{\text{inf}}^{\text{veh}}$ as inputs, **CO³** first transforms the infrastructure point cloud into vehicle-side coordinate, that is $\mathbf{P}'_{\text{inf}} = [T_{\text{inf}}^{\text{veh}}(\mathbf{P}_{\text{inf}}^{\text{xyz}}), \mathbf{P}_{\text{inf}}^{\text{feat}}]$, and concatenates the transformed infrastructure point cloud and the vehicle point cloud $\mathbf{P}_{\text{fusion}} = [\mathbf{P}_{\text{veh}}, \mathbf{P}'_{\text{inf}}]$, where $\mathbf{P}_{\text{fusion}} \in \mathbb{R}^{(N_{\text{veh}}^{\text{p}} + N_{\text{inf}}^{\text{p}}) \times (3+d)}$. Then \mathbf{P}_{veh} and $\mathbf{P}_{\text{fusion}}$ are embedded by the 3D encoder f^{enc}

$$\mathbf{P}_{\text{v/f}}^{\text{enc}} = f^{\text{enc}}(\mathbf{P}_{\text{v/f}}) \quad (1)$$

where $\mathbf{P}_{\text{v/f}}^{\text{enc}} = [\mathbf{P}_{\text{v/f}}^{\text{xyz enc}}, \mathbf{P}_{\text{v/f}}^{\text{feat enc}}]$ and $\mathbf{P}_{\text{v/f}}^{\text{xyz enc}} \in \mathbb{R}^{N_{\text{v/f}}^{\text{p enc}} \times 3}$, $\mathbf{P}_{\text{v/f}}^{\text{feat enc}} \in \mathbb{R}^{N_{\text{v/f}}^{\text{p enc}} \times d^{\text{enc}}}$. $N_{\text{v/f}}^{\text{p enc}}$ is the number of points (or voxels) after encoding. As there exists pooling operations in 3D encoders, the number of points (or voxels) may change when processed by the 3D encoders. d^{enc} is the number of feature channels after encoding. To guide the 3D encoder to learn good representations in an unsupervised manner, we propose a cooperative contrastive loss L_{CO_2} and a contextual shape prediction loss L_{CSP} for optimization. The overall loss function can be written as:

$$L = \sum_{\mathbf{P}_{\text{v/f}} \in \{\mathcal{P}_{\text{v/f}}\}} L_{\text{CO}_2}\{f^{\text{enc}}(\mathbf{P}_{\text{v/f}})\} + w_{\text{CSP}} \times L_{\text{CSP}}\{f^{\text{enc}}(\mathbf{P}_{\text{v/f}}), \mathbf{P}_{\text{veh}}^{\text{xyz}}, \mathbf{P}_{\text{fusion}}^{\text{xyz}}\} \quad (2)$$

where $\mathcal{P}_{\text{v/f}}$ denote a batch of vehicle and fusion point clouds. As described in this equation, L_{CO_2} takes as inputs the encoded vehicle and fusion point clouds and applies contrastive learning on the features of these two views. Meanwhile, L_{CSP} introduces more task-relevant information into f^{enc} by using the encoded features to predict contextual shape whose ground truth is obtained by $\mathbf{P}_{\text{veh}}^{\text{xyz}}$ and $\mathbf{P}_{\text{fusion}}^{\text{xyz}}$. w_{CSP} is a weighting constant that makes the magnitudes of the two loss similar. Details about L_{CO_2} and L_{CSP} will be discussed respectively in Section 3.2 and Section 3.3.

3.2 Cooperative Contrastive Objective

Unsupervised contrastive learning has been demonstrated successful in image domain [1, 2, 3, 4, 5] and indoor-scene point clouds [11, 12, 13]. However, when it turns to outdoor-scene LiDAR point clouds, building adequate views, which share common semantics while differing enough, for contrastive learning is difficult. To tackle this challenge, we utilize a recently released vehicle-infrastructure-cooperation dataset called DAIR-V2X [17] and use vehicle-side point clouds and fusion point clouds as views for contrastive representation learning. The loss is defined as follows:

$$L_{\text{CO}_2} = \frac{1}{N_1} \sum_{n=1}^{N_1} -\log\left(\frac{\exp(z_{\text{veh}}^n \cdot z_{\text{fusion}}^n / \tau)}{\sum_{i=1}^{N_1} \exp(z_{\text{veh}}^i \cdot z_{\text{fusion}}^i / \tau)}\right) \quad \text{with} \quad (3)$$

$$\{z_{\text{v/f}}^n\}_{n=1}^{N_1} \stackrel{\text{sample}}{\sim} Z_{\text{v/f}} \quad ; \quad Z_{\text{v/f}} = \text{normalize}(\text{MLP}_1(\mathbf{P}_{\text{v/f}}^{\text{feat enc}}))$$

where the embedded features of vehicle and fusion point clouds, $\mathbf{P}_{\text{veh}}^{\text{feat enc}}$ and $\mathbf{P}_{\text{fusion}}^{\text{feat enc}}$, are first projected into a common feature space by a Multi-Layer-Perceptron MLP_1 and then normalized. $Z_{\text{v/f}} \in \mathbb{R}^{N_{\text{v/f}}^{\text{p enc}} \times d_1}$ is the projected features of vehicle point cloud and fusion point cloud, where d_1 indicates the dimension of the common feature space and $N_{\text{v/f}}^{\text{p enc}}$ are the point/voxel numbers of encoded vehicle and fusion point clouds respectively. We then sample N_1 pairs of features (z) from $Z_{\text{v/f}}$ for contrastive learning. According to our empirical observation, ground points have a great negative effect on contrastive learning. Thus we mark those points with height value lower than a threshold z_{thd} as ground points and filter them out when sampling. After filtering, we randomly sample N_1 points from the vehicle point cloud and find their corresponding points (or voxels) in the fusion point cloud to form N_1 pairs of points (or voxels). We treat corresponding points (or voxels) as positive pairs and otherwise negative pairs for contrastive learning and the final loss function is shown in the first line of Equation (3), where τ is the temperature parameter.

3.3 Contextual Shape Prediction

CO³ aims to learn representations applicable to various downstream datasets. But the contrastive loss in Eqn.(3) is hard to encode task-relevant information as demonstrated in [18] and the authors resorts to an additional reconstruction objective on image to bring in task-relevant information.

However, for outdoor-scene point clouds, it is extremely difficult to reconstruct the whole scene with point/voxel-level representations. To mitigate this issue, we propose to reconstruct the neighborhood of each point/voxel with its representation. Specifically, a contextual shape prediction loss is designed as below. We describe the process for vehicle features and similar process is applied to fusion ones,

$$L_{CSP} = \frac{1}{N_2} \sum_{n=1}^{N_2} \sum_{m=1}^{N_{bin}} p_{n,m} \log \frac{p_{n,m}}{q_{n,m}} \quad \text{with} \quad (4)$$

$$\{p_{n,*}\}_{n=1}^{N_2} \stackrel{\text{sample}}{\sim} P \quad ; \quad \{q_{n,*}\}_{n=1}^{N_2} \stackrel{\text{sample}}{\sim} Q \quad ; \quad P = \text{softmax}(\text{MLP}_2(\mathbf{P}_{veh}^{\text{feat}^{\text{enc}}}))$$

where the encoded features of vehicle point clouds, $\mathbf{P}_{veh}^{\text{feat}^{\text{enc}}}$, are first passed through another Multi-Layer-Perceptron MLP_2 and softmax operation is applied on the projected features to get a predicted local distribution of each point/voxel, that is $P \in \mathbb{R}^{N_{veh}^{\text{enc}} \times N_{bin}}$. N_{veh}^{enc} is the number of vehicle-side points/voxels after embedded by the 3D encoder and N_{bin} is the number of bin we divide the local neighborhood of each point/voxel. We use $N_{bin} = 32$ in this paper and compute the ‘ground truth’ local shape context $Q \in \mathbb{R}^{N_{veh}^p \times N_{bin}}$ (N_{veh}^p is the number of raw input vehicle points/voxels) beforehand, which will be discussed later. With P and Q , N_2 sampled points/voxels are drawn from P and Q . We have $p_{n,*} \in \mathbb{R}^{N_{bin}}$ and $q_{n,*} \in \mathbb{R}^{N_{bin}}$. Note that these sampled predicted contextual shape distributions are in pairs. Finally, as shown in the first line in Equation (4), L_{CSP} is a KL-divergence loss applied on $p_{n,*}$ and $q_{n,*}$, where the KL-divergence describes the distance between two probability distribution ($p_{n,*}$ and $q_{n,*}$).

To compute the “ground truth” shape context for the i^{th} point/voxel, we first divide the neighborhood of the point/voxel into $N_{bin} = 32$ bins along x-y plane with $R_1 = 0.5m$ and $R_2 = 4m$. Then we compute the number of points/voxels in each bin and this results in $N_{bin} = 32$ numbers $Q_{i,*}^{\text{raw}} \in \mathbb{R}^{N_{bin}}$. Next, $Q_{i,*}$ is finalized as below, where SF_{CSP} is a scaling factor to make the distribution sensible.

$$Q_{i,*} = \text{softmax}(\text{normalize}(Q_{i,*}^{\text{raw}}) \times SF_{CSP}) \quad (5)$$

4 Experiments

4.1 Experiment Setup

Datasets. We utilize the recently released vehicle-infrastructure-cooperation dataset called DAIR-V2X [17] to pre-train 3D sparse encoder with **CO³** and fine-tune the pre-trained encoder on two downstream datasets: *Once* [22] and *KITTI* [35]. **Note** that LiDAR sensors used in *Once* and *KITTI* are **different** than that used in *DAIR-V2X* [17]. Details of the datasets can be found in Appendix C.

Detectors. We select several current state-of-the-art methods implemented in the public repository of *Once* dataset [22]¹ and OpenPCDet² to evaluate the quality of representations learned by **CO³**, including Second [26], CenterPoint [30] and PV-RCNN [32].

Implementation Details of CO³. We use Sparse-Convolution as the 3D encoder which is a 3D convolutional network because it is widely used as 3D encoders in current state-of-the-art methods [26, 30, 32]. We set the number of feature channels $d^{\text{enc}} = 64$, the temperature parameter in contrastive learning $\tau = 0.07$, the dimension of common feature space of vehicle-side and fusion point clouds $d_1 = 256$ and the sample number in cooperative contrastive loss $N_1 = 2048$. For contextual shape prediction, we set the number of bins $N_{bin} = 32$, scaling factor $SF_{CSP} = 4$, the sample number $N_2 = 2048$ and the weighting constant $w_{CSP} = 10$. The threshold for ground point filtering is $z_{\text{thd}} = 1.6\text{m}$.

Baselines. We implement GCC-3D [15] and STRL [16] as baselines. Besides, as proposed in [22], several representation learning methods in image domain and indoor-scene point clouds can be transferred to outdoor scene point clouds, including Swav [3], Deep Cluster [36], BYOL [4] and Point Contrast [11]. All experiment settings for different pre-training methods are the same as **CO³**.

Evaluation Metrics. For *Once* dataset, mAPs (mean accurate precisions) for each category are presented in different ranges while for *KITTI* dataset, all the results are evaluated by mAPs with three difficulty levels: Easy, Moderate and Hard. The results are also further averaged to compute an “Overall” mAP, which is the main evaluation metric.

¹https://github.com/PointsCoder/Once_Benchmark

²<https://github.com/open-mmlab/OpenPCDet>

Init.	Det.	Vehicle			Pedestrian			Cyclist			mAP
		0-30m	30-50m	>50m	0-30m	30-50m	>50m	0-30m	30-50m	>50m	
Rand	Sec.	84.35	66.41	49.49	27.87	23.24	16.36	69.92	52.27	35.25	52.21
Swav		83.21	65.25	50.32	31.55	26.18	17.45	69.40	53.60	35.91	53.03 +0.82
D. Cl.		84.02	67.51	50.26	29.21	21.55	17.39	69.86	51.95	34.69	52.30 +0.09
BYOL		81.60	60.93	46.97	18.71	16.59	12.95	61.20	43.15	27.30	45.24
P.C.		84.19	62.66	46.32	21.55	17.70	14.05	64.98	47.25	28.81	47.64
GCC-3D		85.43	67.88	51.64	27.18	21.55	16.86	72.15	52.28	35.27	52.28
STRL		83.71	65.59	50.39	27.41	22.23	17.17	68.28	51.96	34.17	51.57
Ours		84.62	67.11	49.42	33.64	28.00	17.61	68.22	52.89	32.92	53.28 +1.07
Rand	PV	88.01	72.15	58.93	29.67	23.24	16.47	71.46	54.61	36.60	54.55
Swav		87.80	71.81	57.42	29.86	24.88	17.15	72.56	54.25	36.44	54.89 +0.34
D. Cl.		87.68	71.77	57.11	32.20	26.00	18.28	71.64	53.09	34.80	54.91 +0.36
BYOL		87.37	69.63	55.55	19.74	18.82	14.64	67.01	47.11	31.11	49.41
P.C.		87.72	70.42	55.43	20.52	18.93	16.76	68.58	49.55	33.59	50.49
GCC-3D		87.71	72.20	59.42	27.91	25.96	16.40	72.59	53.88	37.58	54.55
STRL		89.39	70.32	57.40	27.67	23.41	17.55	72.05	54.21	36.85	54.25
Ours		87.85	71.79	57.46	32.75	26.57	17.29	71.22	52.50	36.20	55.17 +0.62
Rand	Cen.	77.42	54.68	38.21	51.08	41.13	25.79	70.67	54.68	35.14	55.92
Swav		77.58	54.28	38.51	53.95	42.52	28.04	71.10	54.99	37.93	57.00
D. Cl.		77.35	55.12	38.91	54.99	42.26	29.31	71.80	56.60	37.05	57.65 +1.08
BYOL		76.56	53.61	37.79	46.48	31.73	18.72	67.55	49.65	27.67	52.17
P.C.		77.64	53.38	39.15	49.69	35.57	23.29	69.37	50.65	30.03	54.17
GCC-3D		77.80	56.75	39.16	54.46	40.11	25.61	74.43	57.04	39.51	58.32 +2.40
STRL		78.01	54.10	39.32	54.09	40.77	25.90	71.60	56.56	36.57	57.44
Ours		78.02	56.13	39.94	55.09	42.34	27.44	74.17	56.05	38.16	58.50 +2.58

Table 1: Results of 3D object detection on Once dataset [22]. We conduct experiments on 3 different detectors: Second [26] (short as Sec.), PV-RCNN [33] (short as PV) and CenterPoint [30] (short as Cen.) and 8 different initialization methods including random (short as Rand, i.e. training from scratch), Swav [3], Deep Cluster (short as D. Cl.) [36], BYOL [4], Point Contrast (short as P.C.) [11], GCC-3D [15] and STRL [16]. Results are mAPs in %. “0-30m”, “30-50m” and “>50m” respectively indicate results for objects in 0 to 30 meters, 30 to 50 meters and 50 meters to infinity. The “mAP” in the final column is the overall evaluation and major metric for comparisons. We use bold font for top 3 mAP in each category in each range for better understanding.

4.2 Main Results

Once Detection. As shown in Table 1, when initialized by CO³, all the three detectors achieve the best performance on the overall mAPs, which we value the most, and CenterPoint [30] achieves the highest overall mAP (58.50) with 2.58 improvement. The improvement on PV-RCNN [33] is 0.62 in mAP (similar lower improvement with other pre-training methods) because PV-RCNN [33] has both the point-based and voxel-based 3D backbones, among which CO³ only pre-trains the voxel-based branch. When we look into detailed categories, it can be found that CO³ achieve consistent improvement on Pedestrian class and the highest mAP when CenterPoint [30] is used as the detector. For Cyclist class, CenterPoint [30] initialized by CO³ achieves the best performance among all the detectors and all the initialization methods. These are important for the deployment of autonomous driving system in real world. For the Vehicle class, the improvement achieved by CO³ is not significant (same in other initialization methods) because the performances of training from scratch are already very high with little room for improvement.

KITTI Detection. As shown in Table 2, when initialized by CO³, PV-RCNN [33] achieves the best performance on Easy and Hard (+1.19) level and third place on Moderate level. Meanwhile Second [26] equipped with CO³ achieves the highest mAP on Easy (+1.11) and Moderate level (+1.22) and third place on Hard level. The lower improvements on KITTI dataset [35] stem from the smaller number of training samples (half of that in Once [22]), which makes the detectors easily reach their capacity and improvement is hard to achieve. Consistent results across different initialization schemes demonstrate this. When we look into detailed categories, CO³ achieve consistent improvement on Pedestrian and Cyclist, which is essential for autonomous driving system.

Overall. CO³ achieve consistent improvement on different detectors and different datasets while other methods only occasionally boost the performance. These demonstrate that the representation learned by CO³, which uses adequate views for contrastive learning and injects task-relevant information via contextual shape prediction, is able to be transferred to different LiDAR sensors.

4.3 Ablation Study

We conduct ablation experiments to analyze the effectiveness of different components in CO³. We respectively pre-train the 3D encoder with cooperative contrastive objective and contextual shape

Init.	Det.	Vehicle	Pedestrian	Cyclist	Overall			
					Easy	Moderate	Hard	
Random	Sec.	77.45	48.71	63.32	73.29	63.16	60.34	
Swav		77.64	49.48	64.95	73.23	64.02^{+0.86}	60.93^{+0.59}	
D. Cl.		77.47	49.46	63.19	73.19	63.37	60.08	
BYOL		76.89	43.29	60.99	71.05	60.39	56.98	
P.C.		77.45	45.32	65.44	72.67	62.74	59.21	
GCC-3D		77.99	47.92	64.45	73.86^{+0.57}	63.45	59.80	
STRL		77.63	48.46	65.52	73.95^{+0.66}	63.87^{+0.71}	60.93^{+0.59}	
Ours		77.95	49.59	65.60	74.40^{+1.11}	64.38^{+1.22}	60.88^{+0.54}	
Random		PV	79.13	53.43	69.12	78.54	67.23	63.68
Swav			79.35	52.92	71.45	78.43^{-0.11}	67.91^{+0.68}	64.60^{+0.92}
D. Cl.	79.22		50.75	71.21	77.05	67.06	64.50^{+0.82}	
BYOL	79.02		51.40	72.07	77.96	67.50	64.42	
P.C.	79.31		51.66	72.40	77.62	67.79^{+0.56}	63.31	
GCC-3D	79.16		50.66	69.95	77.07	66.59	63.67	
STRL	79.15		51.71	67.78	77.10	66.21	62.90	
Ours	79.05		52.47	71.73	78.81^{+0.27}	67.75^{+0.52}	64.87^{+1.19}	

Table 2: Results of 3D object detection on KITTI dataset [35]. Results are mAPs in %. “Easy”, “Moderate” and “Hard” respectively indicate difficulty levels defined in KITTI dataset [35]. Results in each category are from moderate level. The “Overall” results in the final column is the major metric for comparisons. We use bold font for top 3 mAP in each category in each difficulty level for better understanding.

Init.	Once (CenterPoint)				KITTI (Second)			
	Vehicle	Pedestrian	Cyclist	Overall	Vehicle	Pedestrian	Cyclist	Overall
Random	62.85	45.52	59.39	55.92	77.45	48.71	63.32	63.16
Contextual Shape Prediction Only	62.86	49.17	59.86	57.30	77.75	49.16	63.18	63.36
Cooperative Contrastive Only	63.39	48.14	61.05	57.53	77.40	47.78	65.06	63.41
CO³	64.50	48.83	62.17	58.50	77.95	49.59	65.60	64.38

Table 3: Results of ablation study on Once [22] and KITTI [35]. We use CenterPoint [30] on Once and Second [26] on KITTI. Results are mAPs in %. For Once, results are average across different ranges. For KITTI, results are all in moderate level. We highlight the best performance in each column for better understanding.

prediction objective. Then we compare their performance in downstream tasks with those of training from scratch and pre-trained by **CO³**. As shown in Table 3, it can be found that each of the objective alone can achieve slight improvement, which demonstrates the effectiveness of each part of pre-training goal. Besides, once pre-trained by **CO³**, we achieve the best performance.

5 Conclusion and Limitation

In this paper, we propose **CO³**, namely **Cooperative Contrastive Learning** and **Contextual Shape Prediction**, for unsupervised 3D representation learning in outdoor scenes. The recently released vehicle-infrastructure-cooperation dataset DAIR-V2X [17] is utilized to build views for cooperative contrastive learning. Meanwhile the contextual shape prediction objective provides task-relevant information for the 3D encoders. Our experiments demonstrate that the representation learned by **CO³** can be transferred to downstream datasets collected by different LiDAR sensors to improve performance of different detectors. The limitation of our work lies in the relatively small size of the released cooperation dataset. Large-scale dataset is demonstrated useful for unsupervised representation learning in previous works [1, 2, 3, 4, 5]. Thus it will be interesting if larger cooperative datasets can be collected in the future and used for pre-training to see whether larger improvement can be made.

A Background about View Building in Contrastive Learning

In this section, we discuss how to build proper views in contrastive learning. Firstly, we introduce the formulation of contrastive learning and some important properties of good views in contrastive learning as proposed in [14]. Then we discuss view building for LiDAR point clouds.

View Building Contrastive Learning. Unsupervised representation learning aims to pre-train 2D/3D backbones on a dataset without labels, which can be transferred to downstream datasets and tasks to achieve performance improvement over training from scratch (random initialization). Recently, unsupervised contrastive learning achieves great success in image domain [1, 2, 3, 4, 5]. Given a batch of images \mathcal{X} as inputs, these works first apply two kinds of random augmentations for each image $x^n \in \mathcal{X}$ ($n = 1, 2, \dots, N$ where N is the number of images in the batch) to get augmented images x_1^n and x_2^n , which are called different views of x^n . The main objective of contrastive learning is to pull together the representations of views of the same image in the feature space while pushing away representations of different images, as indicated in the equation below:

$$L_{\text{con}} = \frac{1}{N} \sum_{n=1}^N -\log\left(\frac{\exp(z_1^n \cdot z_2^n / \tau)}{\sum_{i=1}^N \exp(z_1^n \cdot z_2^i / \tau)}\right) \quad \text{with} \quad (6)$$

$$z_{1,2}^n = f_1^{\text{enc}}(x_{1,2}^n) \quad n = 1, 2, \dots, N$$

where f_1^{enc} is the 2D backbone used to extract representations. A ResNet50 [37] is usually used for f_1^{enc} because many methods apply it as backbone in downstream tasks including detection [7, 8, 9] and segmentation [7, 38]. **Note** that the ResNet50 is pre-trained only once and used to initialize models in downstream tasks. $z_{1,2}^n$ is the encoded representations for views $I_{1,2}^n$. To apply contrastive loss in the first line in Equation (6), views of the same image are considered as positive pairs and other pairs are negative ones. The numerator indicates the similarity of positive pairs while the denominator sums up the positive similarity and the sum of similarity of negative pairs. τ is the temperature parameter. Minimizing this loss equals to maximize the similarity of positive pairs and minimize the similarity of negative pairs, which is the objective discussed above.

Authors in [14] discuss what property views should have to benefit contrastive learning via Information Theory and propose that mutual information [39, 40, 41] of views $I(x_1^n; x_2^n)$, can indicate the quality of the learned representations. Mutual information formally quantifies “how much information about one random variable we can obtain when observing the other one”. Experiments on images suggest that there exists a “sweet spot” for $I(x_1^n; x_2^n)$ where the pre-trained backbone can achieve the most significant performance improvement in downstream tasks. This means the mutual information between views can neither be too low (sharing little semantics) nor too high (differing little). Further experiments in [14] indicate that the mutual information of different augmented images is high and reducing $I(x_1^n; x_2^n)$ by applying stronger augmentations is effective. The performance on downstream tasks increases at the beginning and then decrease when the augmentations are too strong.

Views Building for LiDAR Point Clouds. As discussed in the main paper, it is impossible for us to reconstruct the whole outdoor-scene for constrative learning, which is demonstrated useful in indoor-scene [11, 12, 13]. And there exists two alternatives to build views for outdoor-scene LiDAR point clouds. The first one ([15]) is to apply data augmentation to single frame of point cloud and treat the original and augmented versions as different views, which is similar to what previous works do in image domain. However, the augmentations in image domain are highly non-linear while all the augmentation of point clouds, including random drop, rotation and scaling, can be implemented in a linear transformation. As claimed in [14], the highly non-linear augmentations on images already bring high mutual information between views. Thus views of LiDAR point clouds built in this way would have higher mutual information, which is not adequate for learning representations. The second intuitive idea to build views is to utilize point clouds at different timestamps, embraced by [16]. However, outdoor-scenes are dynamic and the autonomous driving vehicle has no idea about how other objects (cars, pedestrians, etc.) move. Thus observing one view (timestamp t) bring in little information about the other one (timestamp $t+10$ for example), meaning that $I(x_1^n; x_2^n)$ can be extremely low and this can be harmful to the learned representations. Due to these limitations, pre-trained 3D encoders in [15, 16] cannot achieve noticeable improvement when transferring to datasets collected by different LiDAR sensors. Thus, in this paper, we propose to utilize the vehicle-infrastructure-cooperation dataset [17], which capture the same scene from different view-point at the same timestamp, for contrastive representation learning. Views built with this dataset neither share

too much information (captured from different view-points) nor share too little information (captured at the same time, easy to find correspondence), which is adequate for contrastive learning.

B Reconstruction Objective for Task-relevant Information

In this section, we borrow the ideas from [18] to explain why pure contrastive learning bring less improvements as shown in Table 3 in the main paper. Firstly, we give the definition of sufficient representation and minimal sufficient representation in contrastive learning. Then, we present analysis on image classification problem as downstream task and we refer readers to [18] for other downstream tasks. Finally, we propose our pre-training objective for LiDAR point clouds.

Sufficient Representation and Minimal Sufficient Representation. Sufficient Representation $z_{1,\text{suf}}^n$ of x_1^n contains all the information that is shared by x_1^n and x_2^n , which means $z_{1,\text{suf}}^n$ can be used to express common semantics shared by these two views. Among all the sufficient representations for x_2^n , minimal sufficient representation $z_{1,\text{min}}^n$ contains the least information about x_1^n . The learned representation in contrastive learning is sufficient and almost minimal. Assuming that $\mathcal{Z}_{1,\text{suf}}$ is the set of all possible sufficient representations, we can define these two concepts as follows

Definition 1. $z_{1,\text{suf}}^n$ of view x_1^n is sufficient for x_2^n **if and only if** $I(z_{1,\text{suf}}^n, x_2^n) = I(x_1^n, x_2^n)$.

Definition 2. $z_{1,\text{min}}^n \in \mathcal{Z}_{1,\text{suf}}$ of view x_1^n is minimal sufficient **if and only if** $I(z_{1,\text{min}}^n, x_1^n) \leq I(z_{1,\text{suf}}^n, x_1^n), \forall z_{1,\text{suf}}^n \in \mathcal{Z}_{1,\text{suf}}$.

Theorem. (1) $z_{1,\text{suf}}$ provides more information about the downstream task T than $z_{1,\text{min}}$. (2) The upper bound of error rates in downstream tasks using minimal sufficient representations are higher than that of sufficient representations. That is,

$$\begin{aligned} I(z_{1,\text{suf}}, T) &\geq I(z_{1,\text{min}}, T) \\ \sup\{P_{\text{suf}}^e\} &\leq \sup\{P_{\text{min}}^e\} \end{aligned} \quad (7)$$

This gap stems from the missing task-relevant information in $z_{1,\text{min}}$. To prevent this problem, authors in [18] propose to add a reconstruction objective (reconstruct x_1 using z_1) alongside the contrastive loss to increase $I(z_1, x_1)$, which indirectly increases $I(z_1, T|x_2)$ and brings improvement in downstream classification problem over pure contrastive learning.

Proof for Image Classification Problem. We denote the downstream classification task as T and the task-relevant information in minimal sufficient representation $z_{1,\text{min}}$ can be described as below:

$$\begin{aligned} I(z_{1,\text{suf}}, T) &= I(z_{1,\text{min}}, T) + [I(x_1, T|z_{1,\text{min}}) - I(x_1, T|z_{1,\text{suf}})] \\ &\geq I(z_{1,\text{min}}, T) \end{aligned} \quad (8)$$

To begin with, $z_{1,\text{suf}}$ and $z_{1,\text{min}}$ are sufficient representations and they contain two parts of information: shared information between x_1 and x_2 , I_{share} , and extra information about x_1 , $I_{\text{suf}} > I_{\text{min}}$. Thus the mutual information $I(z_{1,\text{suf}}, T)$ can be decomposed into $I(z_{1,\text{min}}, T)$ and $[I(x_1, T|z_{1,\text{min}}) - I(x_1, T|z_{1,\text{suf}})]$, where $I(x_1, T|z_{1,\text{min}})$ indicates the information about T we can obtain by observing x_1 when $z_{1,\text{min}}$ is known. As the second term is larger than zero ($I_{\text{suf}} > I_{\text{min}}$), the right-hand-side of the first line in Equation (8) is larger than $I(z_{1,\text{min}}, T)$, which indicates that $z_{1,\text{suf}}$ contains more task-relevant information than $z_{1,\text{min}}$ and thus would have better performance in T . Then we consider using Bayes error rate P^e [42], which is the lower-bound of achievable error for the classifier, to analysis performance of $z_{1,\text{suf}}$ and $z_{1,\text{min}}$ on downstream classification problem. We have

$$\begin{aligned} P_{\text{suf}}^e &\leq 1 - \exp[-H(T) + I(x_1, x_2, T) + I(z_{1,\text{suf}}, T|x_2)] \\ P_{\text{min}}^e &\leq 1 - \exp[-H(T) + I(x_1, x_2, T)] \end{aligned} \quad (9)$$

where $H(T)$ is the entropy of the task. Since $1 - \exp[-(H(T) + I(x_1, x_2, T) + I(z_{1,\text{suf}}, T|x_2))] \leq 1 - \exp[-H(T) + I(x_1, x_2, T)]$, the upper bound of Bayes error rate of minimal sufficient representation is larger than that of sufficient representations. This indicates that ideally $z_{1,\text{suf}}$ can achieve better performance than $z_{1,\text{min}}$ in classification problem.

Contextual Shape Prediction Objective. As it is impossible to reconstruct the whole scene point cloud with point-level or voxel-level representations. We propose an additional pre-training objective to predict distribution of local neighborhood of a point/voxel using point/voxel-level representation.

We use shape context to describe distribution of local neighborhood of a point/voxel, which has been demonstrated as a useful local distribution descriptor in previous works [12, 19, 20, 21]. As demonstrated in our ablation study (Table 3 in main paper), this additional pre-training objective bring more significant performance improvement over pre-trained by pure contrastive loss. We also provide python-style code for computing shape context as followings

Algorithm 1 Implementation of Contextual Shape Computation in Python Style.

```

class Contextual_Shape(object):
    def __init__(self, r1=0.125, r2=2, nbins_xy=2, nbins_zy=2):
        self.r1 = r1
        self.r2 = r2
        self.nbins_xy = nbins_xy
        self.nbins_zy = nbins_zy
        self.partitions = nbins_xy * nbins_zy * 2

    def pdist_batch(rel_trans):
        D2 = torch.sum(rel_trans.pow(2), 3)
        return torch.sqrt(D2 + 1e-7)

    def compute_rel_trans_batch(A, B):
        return A.unsqueeze(1) - B.unsqueeze(2)

    def hash_batch(A, B, seed):
        mask = (A >= 0) & (B >= 0)
        C = torch.zeros_like(A) - 1
        C[mask] = A[mask] * seed + B[mask]
        return C

    def compute_angles_batch(rel_trans):
        angles_xy = torch.atan2(rel_trans[:, :, :, 1], rel_trans[:, :, :, 0])
        angles_xy = torch.fmod(angles_xy + 2 * math.pi, 2 * math.pi)
        angles_zy = torch.atan2(rel_trans[:, :, :, 1], rel_trans[:, :, :, 2])
        angles_zy = torch.fmod(angles_zy + 2 * math.pi, math.pi)
        return angles_xy, angles_zy

    def compute_partitions_batch(self, xyz_batch):
        rel_trans_batch = ShapeContext.compute_rel_trans_batch(xyz_batch, xyz_batch)
        # compute angles from different points to the query one
        angles_xy_batch, angles_zy_batch = ShapeContext.compute_angles_batch(
            rel_trans_batch)
        angles_xy_bins_batch = torch.floor(angles_xy_batch / (2 * math.pi / self.
            nbins_xy))
        angles_zy_bins_batch = torch.floor(angles_zy_batch / (math.pi / self.
            nbins_zy))
        angles_bins_batch = ShapeContext.hash_batch(angles_xy_bins_batch,
            angles_zy_bins_batch, self.nbins_zy)
        # compute distances between different points and the query one
        distance_matrix_batch = ShapeContext.pdist_batch(rel_trans_batch)
        dist_bins_batch = torch.zeros_like(angles_bins_batch) - 1
        # generate partitions for each points
        mask_batch = (distance_matrix_batch >= self.r1) & (distance_matrix_batch <
            self.r2)
        dist_bins_batch[mask_batch] = 0
        mask_batch = distance_matrix_batch >= self.r2
        dist_bins_batch[mask_batch] = 1
        bins_batch = ShapeContext.hash_batch(dist_bins_batch, angles_bins_batch,
            self.nbins_xy * self.nbins_zy)
        return bins_batch

```

C Datasets Details

In this section, we introduce details about different datasets used in the main paper for evaluation and also two more datasets in additional experiments.

DAIR-V2X. *DAIR-V2X* [17] is the first real-world autonomous dataset for vehicle-infrastructure-cooperative detection task. It covers various scenes, including cities and highways, and different weather condition including sunny, rainy and foggy days. A virtual world coordinate is used to align the vehicle LiDAR coordinate and infrastructure LiDAR coordinate. There are 38845 LiDAR frames (10084 in vehicle-side and 22325 in infrastructure-side) for cooperative-detection task. The dataset contains around 7000 synchronized cooperative samples in total and we utilize them to pre-train 3D encoder in an unsupervised manner via the proposed **CO³**. The LiDAR sensor at vehicle-side is 40-beam while a 120-beam LiDAR is utilized at infrastructure-side.

Once. *Once* [22] is a large-scale autonomous dataset for evaluating self-supervised methods with 1 Million LiDAR frames and only 15k fully annotated frames with 3 classes (Vehicle, Pedestrian, Cyclist). A 40-beam LiDAR is used in [22] to collect the point cloud data. We adopt common practice, including point cloud range and voxel size, in their public code repository³. As for the evaluation metrics, IoU thresholds 0.7, 0.3, 0.5 are respectively adopted for vehicle, pedestrian, cyclist. Then 50 score thresholds with the recall rates ranging from 0.02 to 1.00 (step size if 0.02) are computed and the 50 corresponding values are used to draw a PR curve, resulting in the final mAPs (mean accurate precisions) for each category. We also further overage over the three categories and compute an 'Overall' mAP for evaluations.

KITTI. *KITTI* [35] is a widely used self-driving dataset, where point clouds are collected by LiDAR with 64 beams. It contains around 7k samples for training and another 7k for evaluation. For point cloud range and voxel size, we adopt common practice in current popular codebase like MMDetection3D⁴ and OpenPCDet⁵. All the results are evaluated by mAPs with three difficulty levels: Easy, Moderate and Hard. These three results are further average and an 'Overall' mAP is generated for comparisons.

Waymo. *Waymo* [43] is a large-scale dataset for evaluating 3D object detection methods. This dataset contains more than 200K frames of outdoor-scene point clouds, among which 150K are for training and others are for validation and testing. The LiDAR used to collect this dataset is 64-beam. For point cloud range and voxel size, we adopt common practice in OpenPCDet. We evaluate the models in Waymo by mean average precision (short as AP) and mean average precision with heading (short as APH) at two difficulty level defined in [43]: Level 1 and 2.

NuScenes. *NuScenes* [44] dataset contains around 1.4M annotated 3D boxes and the scenes are split in 700/150/150 respectively for training/validation/testing. The LiDAR used to collect this dataset is 32-beam. For point cloud range and voxel size, we adopt common practice in OpenPCDet. We evaluate the models in NuScenes by mean average precision (short as mAP) in each annotated category including Car, Construction Vehicle, Bus, Trailer, Barrier, Motorcycle, Pedestrian and Traffic Cone. We further average performance in each category and error in translation and rotation, which generate "mAP" and "NDS" (NuScenes Detection Scores) metrics for overall evaluation.

D Additional Experiment Results

D.1 Sample Efficiency Results

The main goal of unsupervised representation learning is to reduce labels required in downstream tasks. We further evaluate the proposed **CO³** in two large-scale autonomous datasets *Waymo* [43] and *NuScenes* [44] in a sample efficiency aspect. We use only 1% data in both datasets to conduct the fine-tuning experiments. Second [26] (short as Sec.) and CenterPoint [30] (short as Cen.) are used in both datasets. For evaluation details in both datasets, please refer to C. We include four kinds of initialization schemes in our experiments including Rand (random initialization), GCC (GCC-3D from [15]), STRL from [16] and our proposed **CO³** ("Ours"). **Note** that we only pre-train **CO³** once on *DAIR-V2X* [17] and use the pre-trained backbone for downstream tasks in four different datasets (*KITTI* [35], *Once* [22], *Waymo* [43] and *NuScenes* [44]).

Sample Efficiency in Waymo Dataset [43]. As shown in Table 4, when initialized by **CO³**, both detectors achieve the best performance on the overall mAPs and mAPHs, which we value the most.

³https://github.com/PointsCoder/Once_Benchmark

⁴<https://github.com/open-mmlab/mmdetection3d>

⁵<https://github.com/open-mmlab/OpenPCDet>

When we look into detailed categories, it can be found that **CO³** achieve consistent improvement on all the classes and the highest mAPs and mAPHs when CenterPoint [30] is used as the detector. These are important for real-world deployment of autonomous driving system when labels are scarce.

Init.	Det.	Vehicle		Pedestrian		Cyclist		Overall	
		Level 1 AP/APH	Level 2 AP/APH	Level 1 AP/APH	Level 2 AP/APH	Level 1 AP/APH	Level 2 AP/APH	Level 1 AP/APH	Level 2 AP/APH
Rand	Sec.	52.83/51.37	45.98/44.69	45.04/22.86	38.33/19.45	32.72/20.88	31.46/20.08	43.53/31.70	38.59/28.07
GCC		53.18/51.72	46.40/45.11	45.90/22.81	39.38/19.58	36.85 /20.66	35.45 /19.87	45.31/31.73	40.41/28.19
STRL		51.79/50.34	44.84/43.58	43.58/23.05	37.02/19.58	32.22/18.96	30.98/18.23	42.53/30.78	37.61/27.13
Ours		54.50/53.17	47.48/46.31	46.72/25.50	40.06/21.86	35.60/23.16	34.25/22.29	45.64/33.94	40.60/30.15
								+2.11/+2.24	+2.01/+2.08
Rand	Cen.	53.36/52.57	46.49/45.79	50.10/42.47	43.21/36.59	49.73/48.38	47.83/46.53	51.06/47.81	45.84/42.97
GCC		53.38/52.60	46.51/45.82	50.23/42.05	43.58/36.44	48.12/46.69	46.30/44.92	50.58/47.11	45.46/42.39
STRL		52.40/51.59	45.43/44.73	49.05/41.07	42.36/35.43	48.31/46.65	46.49/44.88	49.92/46.43	46.30/43.47
Ours		54.21/53.47	47.25/46.60	50.44/42.84	43.75/37.11	49.80/48.55	47.89/46.69	51.48/48.29	46.30/43.47
								+0.42/+0.48	+0.46/+0.50

Table 4: Results of sample efficiency experiments on Waymo dataset [43]. We conduct experiments on 2 different detectors: Second [26] (short as Sec.) and CenterPoint [30] (short as Cen.) and 4 different initialization methods including random (short as Rand, i.e. training from scratch), GCC-3D [15], STRL [16] and the proposed **CO³**. Results are mAPs and mAPHs in %. The “mAP” in the final column is the overall evaluation and major metric for comparisons. We use bold font for the best performance in each category for better understanding.

Sample Efficiency in Nuscenes Dataset [44]. As shown in Table 5, when initialized by **CO³**, both detectors achieve the best performance on the overall mAPs and NDS, which we value the most. When we look into detailed categories, it can be found that **CO³** achieve consistent improvement on all the classes and when initialized by **CO³**, we achieve the highest mAPs in 6 categories (car, truck, construction vehicle, bus, pedestrian and traffic cone). These results demonstrate that **CO³** can be used to improve the performance of different detectors in a sample-efficient setting (small number of labelled data), which is important for the deployment of autonomous driving vehicle in real world.

Init.	Det.	Car	Truck	C. V.	Bus	Trailer	Barrier	M. C.	Ped.	T. C.	mAP	NDS
Rand	Sec.	53.28	18.53	2.17	25.55	5.44	14.66	2.35	37.16	13.41	17.25	28.28
GCC		49.36	15.14	1.83	23.87	3.93	16.61	0.91	47.18	17.38	17.62	27.14
STRL		53.94	18.76	1.88	27.89	7.79	17.38	2.17	37.83	14.17	18.18	29.62
Ours		57.35	19.78	4.33	30.47	5.80	17.35	3.00	44.30	16.04	19.84^{+2.59}	30.83^{+2.55}
Rand	Cen.	59.21	16.19	1.92	19.57	3.14	34.65	10.10	53.71	27.84	22.64	30.58
GCC		61.05	17.10	3.75	22.24	3.99	37.13	12.85	55.52	26.10	24.02	31.53
STRL		57.03	14.13	2.21	17.14	2.66	32.31	5.95	55.64	25.76	21.28	29.80
Ours		61.31	18.46	2.97	22.97	4.38	35.02	10.19	55.75	31.44	24.25^{+1.61}	31.55^{+0.97}

Table 5: Results of sample efficiency experiments on NuScenes dataset [44]. We conduct experiments on 2 different detectors: Second [26] (short as Sec.) and CenterPoint [30] (short as Cen.) and 4 different initialization methods including random (short as Rand, i.e. training from scratch), GCC-3D [15], STRL [16] and the proposed **CO³**. Results are mAPs in %. Results in 9 classes are shown including construction vehicle (short as C. V.), motorcycle (short as M. C.), pedestrian (short as Ped.) and traffic cone (short as T. C.). The “mAP” and “NDS” in the last two column are major metrics for comparisons. We use bold font for the best performance in each category for better understanding.

E Implementation Details

In this section, we introduce some details about implementation in both pre-training stage and fine-tuning stage. Common settings of pre-training and fine-tuning are listed in Table 6 and we discuss other settings that vary in different detectors later.

Other Pre-training Settings. To accelerate the pre-training process, we utilize the “repeated dataset” in MMDetection3D and the schedule is set to 10 epochs, which equals to 20 epochs without “repeated dataset”. Thus the number 20 for training epochs in Table 6 is tilt.

Other Fine-tuning Settings. Batch size settings for different detectors on different datasets are shown in Table 7. We train 20 epochs for CenterPoint [30] in NuScenes [44] and 80 epochs for Second [26] in Nuscenes [44]. We use different types of GPUs, different number of GPUs and different version of PyTorch [45] as compared to those used in the codebases, which may lead to degrading when training from scratch. Thus these parameters are tuned based on the original settings

Configuration	Pre-training	KITTI	Once	Waymo	NuScenes
optimizer	AdamW	Adam	Adam	Adam	Adam
base learning rate	0.0001	0.003	0.003	0.003	0.003
weight decay	0.01	0.01	0.01	0.01	0.01
batch size	16	-	-	-	-
learning rate schedule	cyclic	cyclic	cyclic	cyclic	cyclic
GPU numbers	8	4	4	8	8
training epochs	20	80	80	30	-

Table 6: Details about implementations. “Pre-training” means settings in *DAIR-V2X* [17]. “KITTI”, “Once”, “Waymo” and “NuScenes” respectively indicate settings for detection tasks in *KITTI* [35], *Once* [22], *Waymo* [43] and *NuScenes* [44]. We list all common settings and discuss those vary in different detectors below, which are marked as “-” in this table.

from the codebases to make the performance of training from scratch match or even surpass the results they published.

Detectors	KITTI	Once	Waymo	NuScenes
Second	48	48	48	32
PV-RCNN	16	48	-	-
CenterPoint	-	32	32	32

Table 7: Details about batchsize settings for different detectors on different datasets. “-” means there is no configuration for the detector on the exact dataset in the codebase or we do not conduct the downstream experiments.

References

- [1] K. He, H. Fan, Y. Wu, S. Xie, and R. Girshick. Momentum contrast for unsupervised visual representation learning. In *Proceedings of the IEEE/CVF Conference on Computer Vision and Pattern Recognition*, pages 9729–9738, 2020.
- [2] Y. Tian, D. Krishnan, and P. Isola. Contrastive multiview coding. *arXiv preprint arXiv:1906.05849*, 2019.
- [3] M. Caron, I. Misra, J. Mairal, P. Goyal, P. Bojanowski, and A. Joulin. Unsupervised learning of visual features by contrasting cluster assignments. In H. Larochelle, M. Ranzato, R. Hadsell, M. F. Balcan, and H. Lin, editors, *Advances in Neural Information Processing Systems*, volume 33, pages 9912–9924. Curran Associates, Inc., 2020. URL <https://proceedings.neurips.cc/paper/2020/file/70feb62b69f16e0238f741fab228fec2-Paper.pdf>.
- [4] J.-B. Grill, F. Strub, F. Altché, C. Tallec, P. Richemond, E. Buchatskaya, C. Doersch, B. Avila Pires, Z. Guo, M. Gheshlaghi Azar, B. Piot, k. kavukcuoglu, R. Munos, and M. Valko. Bootstrap your own latent - a new approach to self-supervised learning. In H. Larochelle, M. Ranzato, R. Hadsell, M. F. Balcan, and H. Lin, editors, *Advances in Neural Information Processing Systems*, volume 33, pages 21271–21284. Curran Associates, Inc., 2020. URL <https://proceedings.neurips.cc/paper/2020/file/f3ada80d5c4ee70142b17b8192b2958e-Paper.pdf>.
- [5] X. Wang, R. Zhang, C. Shen, T. Kong, and L. Li. Dense contrastive learning for self-supervised visual pre-training. In *Proc. IEEE Conf. Computer Vision and Pattern Recognition (CVPR)*, 2021.
- [6] J. Deng, W. Dong, R. Socher, L.-J. Li, K. Li, and L. Fei-Fei. Imagenet: A large-scale hierarchical image database. In *2009 IEEE Conference on Computer Vision and Pattern Recognition*, pages 248–255, 2009. doi:10.1109/CVPR.2009.5206848.
- [7] R. Girshick, J. Donahue, T. Darrell, and J. Malik. Rich feature hierarchies for accurate object detection and semantic segmentation. In *Proceedings of the IEEE conference on computer vision and pattern recognition*, pages 580–587, 2014.

- [8] T.-Y. Lin, P. Dollár, R. Girshick, K. He, B. Hariharan, and S. Belongie. Feature pyramid networks for object detection. In *Proceedings of the IEEE conference on computer vision and pattern recognition*, pages 2117–2125, 2017.
- [9] S. Ren, K. He, R. Girshick, and J. Sun. Faster r-cnn: Towards real-time object detection with region proposal networks. *Advances in neural information processing systems*, 28, 2015.
- [10] L. Zhang and Z. Zhu. Unsupervised feature learning for point cloud understanding by contrasting and clustering using graph convolutional neural networks. In *2019 International Conference on 3D Vision (3DV)*, pages 395–404. IEEE, 2019.
- [11] S. Xie, J. Gu, D. Guo, C. R. Qi, L. Guibas, and O. Litany. Pointcontrast: Unsupervised pre-training for 3d point cloud understanding. In *European Conference on Computer Vision*, pages 574–591. Springer, 2020.
- [12] J. Hou, B. Graham, M. Nießner, and S. Xie. Exploring data-efficient 3d scene understanding with contrastive scene contexts. In *Proceedings of the IEEE/CVF Conference on Computer Vision and Pattern Recognition*, pages 15587–15597, 2021.
- [13] Y. Liu, L. Yi, S. Zhang, Q. Fan, T. Funkhouser, and H. Dong. P4contrast: Contrastive learning with pairs of point-pixel pairs for rgb-d scene understanding. *arXiv preprint arXiv:2012.13089*, 2020.
- [14] Y. Tian, C. Sun, B. Poole, D. Krishnan, C. Schmid, and P. Isola. What makes for good views for contrastive learning? In H. Larochelle, M. Ranzato, R. Hadsell, M. F. Balcan, and H. Lin, editors, *Advances in Neural Information Processing Systems*, volume 33, pages 6827–6839. Curran Associates, Inc., 2020. URL <https://proceedings.neurips.cc/paper/2020/file/4c2e5eaae9152079b9e95845750bb9ab-Paper.pdf>.
- [15] H. Liang, C. Jiang, D. Feng, X. Chen, H. Xu, X. Liang, W. Zhang, Z. Li, and L. Van Gool. Exploring geometry-aware contrast and clustering harmonization for self-supervised 3d object detection. In *Proceedings of the IEEE/CVF International Conference on Computer Vision*, pages 3293–3302, 2021.
- [16] S. Huang, Y. Xie, S.-C. Zhu, and Y. Zhu. Spatio-temporal self-supervised representation learning for 3d point clouds. In *Proceedings of the IEEE/CVF International Conference on Computer Vision*, pages 6535–6545, 2021.
- [17] H. Yu, Y. Luo, M. Shu, Y. Huo, Z. Yang, Y. Shi, Z. Guo, H. Li, X. Hu, J. Yuan, and Z. Nie. Dair-v2x: A large-scale dataset for vehicle-infrastructure cooperative 3d object detection. In *IEEE/CVF Conf. on Computer Vision and Pattern Recognition (CVPR)*, June 2022.
- [18] H. Wang, X. Guo, Z.-H. Deng, and Y. Lu. Rethinking minimal sufficient representation in contrastive learning. *arXiv preprint arXiv:2203.07004*, 2022.
- [19] S. Belongie, J. Malik, and J. Puzicha. Shape matching and object recognition using shape contexts. *IEEE transactions on pattern analysis and machine intelligence*, 24(4):509–522, 2002.
- [20] M. Körtgen, G.-J. Park, M. Novotni, and R. Klein. 3d shape matching with 3d shape contexts. In *The 7th central European seminar on computer graphics*, volume 3, pages 5–17. Citeseer, 2003.
- [21] S. Xie, S. Liu, Z. Chen, and Z. Tu. Attentional shapecontextnet for point cloud recognition. In *Proceedings of the IEEE Conference on Computer Vision and Pattern Recognition*, pages 4606–4615, 2018.
- [22] J. Mao, M. Niu, C. Jiang, X. Liang, Y. Li, C. Ye, W. Zhang, Z. Li, J. Yu, C. Xu, et al. One million scenes for autonomous driving: Once dataset. 2021.
- [23] S. Shi, X. Wang, and H. Li. Pointcnn: 3d object proposal generation and detection from point cloud. In *The IEEE Conference on Computer Vision and Pattern Recognition (CVPR)*, June 2019.

- [24] X. Chen, H. Ma, J. Wan, B. Li, and T. Xia. Multi-view 3d object detection network for autonomous driving. In *Proceedings of the IEEE conference on Computer Vision and Pattern Recognition*, pages 1907–1915, 2017.
- [25] B. Yang, W. Luo, and R. Urtasun. Pixor: Real-time 3d object detection from point clouds. In *Proceedings of the IEEE conference on Computer Vision and Pattern Recognition*, pages 7652–7660, 2018.
- [26] Y. Zhou and O. Tuzel. Voxelnet: End-to-end learning for point cloud based 3d object detection. In *Proceedings of the IEEE Conference on Computer Vision and Pattern Recognition*, pages 4490–4499, 2018.
- [27] A. H. Lang, S. Vora, H. Caesar, L. Zhou, J. Yang, and O. Beijbom. Pointpillars: Fast encoders for object detection from point clouds. In *Proceedings of the IEEE/CVF Conference on Computer Vision and Pattern Recognition*, pages 12697–12705, 2019.
- [28] H. Su, S. Maji, E. Kalogerakis, and E. Learned-Miller. Multi-view convolutional neural networks for 3d shape recognition. In *Proceedings of the IEEE international conference on computer vision*, pages 945–953, 2015.
- [29] S. Shi, Z. Wang, J. Shi, X. Wang, and H. Li. From points to parts: 3d object detection from point cloud with part-aware and part-aggregation network. *IEEE transactions on pattern analysis and machine intelligence*, 43(8):2647–2664, 2020.
- [30] T. Yin, X. Zhou, and P. Krahenbuhl. Center-based 3d object detection and tracking. In *Proceedings of the IEEE/CVF conference on computer vision and pattern recognition*, pages 11784–11793, 2021.
- [31] L. Fan, Z. Pang, T. Zhang, Y.-X. Wang, H. Zhao, F. Wang, N. Wang, and Z. Zhang. Embracing single stride 3d object detector with sparse transformer. *arXiv preprint arXiv:2112.06375*, 2021.
- [32] S. Shi, C. Guo, L. Jiang, Z. Wang, J. Shi, X. Wang, and H. Li. Pv-rcnn: Point-voxel feature set abstraction for 3d object detection. In *Proceedings of the IEEE Conference on Computer Vision and Pattern Recognition*, 2020.
- [33] S. Shi, L. Jiang, J. Deng, Z. Wang, C. Guo, J. Shi, X. Wang, and H. Li. Pv-rcnn++: Point-voxel feature set abstraction with local vector representation for 3d object detection. *arXiv preprint arXiv:2102.00463*, 2021.
- [34] J. Deng, S. Shi, P. Li, W. Zhou, Y. Zhang, and H. Li. Voxel r-cnn: Towards high performance voxel-based 3d object detection. In *Proceedings of the AAAI Conference on Artificial Intelligence*, volume 35, pages 1201–1209, 2021.
- [35] A. Geiger, P. Lenz, and R. Urtasun. Are we ready for autonomous driving? the kitti vision benchmark suite. In *Conference on Computer Vision and Pattern Recognition (CVPR)*, 2012.
- [36] M. Caron, P. Bojanowski, A. Joulin, and M. Douze. Deep clustering for unsupervised learning of visual features. In *Proceedings of the European conference on computer vision (ECCV)*, pages 132–149, 2018.
- [37] K. He, X. Zhang, S. Ren, and J. Sun. Deep residual learning for image recognition. In *Proceedings of the IEEE conference on computer vision and pattern recognition*, pages 770–778, 2016.
- [38] L.-C. Chen, G. Papandreou, I. Kokkinos, K. Murphy, and A. L. Yuille. Deeplab: Semantic image segmentation with deep convolutional nets, atrous convolution, and fully connected crfs. *IEEE transactions on pattern analysis and machine intelligence*, 40(4):834–848, 2017.
- [39] C. E. Shannon. A mathematical theory of communication. *ACM SIGMOBILE mobile computing and communications review*, 5(1):3–55, 2001.
- [40] J. Kreer. A question of terminology. *IRE Transactions on Information Theory*, 3(3):208–208, 1957. doi:10.1109/TIT.1957.1057418.

- [41] Wikipedia contributors. Mutual information — Wikipedia, the free encyclopedia, 2022. URL https://en.wikipedia.org/w/index.php?title=Mutual_information&oldid=1089343634. [Online; accessed 21-June-2022].
- [42] K. Fukunaga. *Introduction to statistical pattern recognition*. Elsevier, 2013.
- [43] P. Sun, H. Kretzschmar, X. Dotiwalla, A. Chouard, V. Patnaik, P. Tsui, J. Guo, Y. Zhou, Y. Chai, B. Caine, et al. Scalability in perception for autonomous driving: Waymo open dataset. In *Proceedings of the IEEE/CVF conference on computer vision and pattern recognition*, pages 2446–2454, 2020.
- [44] H. Caesar, V. Bankiti, A. H. Lang, S. Vora, V. E. Liong, Q. Xu, A. Krishnan, Y. Pan, G. Baldan, and O. Beijbom. nuscenes: A multimodal dataset for autonomous driving. In *Proceedings of the IEEE/CVF conference on computer vision and pattern recognition*, pages 11621–11631, 2020.
- [45] A. Paszke, S. Gross, F. Massa, A. Lerer, J. Bradbury, G. Chanan, T. Killeen, Z. Lin, N. Gimelshein, L. Antiga, et al. Pytorch: An imperative style, high-performance deep learning library. *Advances in neural information processing systems*, 32, 2019.